# Theoretical Prediction of Half-Metallic Properties of CrHfCoZ (Z = Ga, In, Tl, Si) Alloys

Xiao-Ping Wei[a,*], Tie-Yi Cao[a], Peifeng Gao[b] and Xiao-Wei Sun[a]

[a] *The School of Mathematics and Physics, Lanzhou Jiaotong University, Lanzhou 730070, P.R. China*
[b] *Key Laboratory of Mechanics on Western Disaster and Environment, Ministry of Education, College of Civil Engineering and Mechanic, Key Laboratory of Special Function Materials and Structure Design of Ministry of Education, Lanzhou University, Lanzhou 730000, P.R. China*

Received: 11.02.2020 & Accepted: 09.04.2020

Doi: 10.12693/APhysPolA.138.440 *e-mail: weixp2008@lzjtu.edu.cn

Using first-principles calculations, we investigate systematically the stability, electronic and magnetic characteristics for the CrHfCoZ (Z = Ga, In, Tl, Si) alloys. Stability is estimated in views of thermodynamics, mechanical and dynamics points. Electronic calculations show that CrHfCoZ alloys have half-metallic behavior, and their integral magnetic moments obey the Slater–Pauling rule. Further, we discuss the formation of spin-flip gap along with integer magnetic moment according to the density of states. In addition, we plot the Fermi surface to illustrate the electronic behavior around the Fermi level of CrHfCoZ alloys. Finally, the changes of conduction band maximum and valence band minimum dependent on the lattice constants are also discussed. Our research may provide a potential applications in spintronic devices.

topics: quaternary Heusler alloys, half-metallicity, electronic structure, magnetic properties

## 1. Introduction

Recently, the nanoelectronics and spintronics have attracted widely attention for the designing new materials for building blocks of nanoscale electronic devices. Consequently, the spintronics combined magnetic with semiconductor is of magnetoelectronics. Especially, the half-metallic alloys, which play a key role in spintronic devices, exhibit metallic nature for one spin channel while a semiconducting or insulator behavior is observed in opposite spin channel, and then leading to the fully spin polarization for density of states at the Fermi level, thus generating a fully spin-polarized current as spin polarized injected source. Initially, De Groot et al. predict the first half-metallic alloy by using electronic structure calculations [1]. Since then, many half-metals are predicted successively in theory, including transition metal oxide [2–5], double perovskites [6–9], MXenes [10–16] and the Heusler alloys [17–28], etc. Among them, the Heusler alloys with matched structure with semiconductor attract widely attention.

At present, much effort focuses on the quaternary Heusler alloys XX'YZ with structural prototype LiMgPdSn [29, 30], where the XX'YZ is usually obtained by substituting the X' for X in full-Heusler alloys $X_2YZ$. Similar with the full-Heusler alloys, the striking feature of quaternary Heusler alloys is also their half-metallic behavior. So far, the half-metallic or spin gapless semiconducting behaviors are observed in many quaternary Heusler alloys with $3d$ elements [31–39]. Yet quaternary Heusler compounds containing $f$ electrons are not reported. In order to further design and develop, half-metallic quaternary Heusler alloys should meet the demand of spintronic applications. In the present work, new quaternary Heusler alloys CrHfCoZ (Z = Ga, In, Tl, Si) including $f$ electrons are designed, and we study systematically their stability, electronic and magnetic properties by using electronic structure calculations.

## 2. Calculation details

All calculations are carried out by employing full-potential local-orbital minimum-basis method [40, 41]. In this scheme, the site-centered potentials and densities were expanded in spherical harmonic contributions up to $l_{\max} = 12$, the exchange-correlation (XC) potential is applied, the Perdew–Burke–Ernzerhof within the generalized gradient approximation (GGA) [42]. A $20 \times 20 \times 20$ $\boldsymbol{k}$-mesh in the Brillouin zone is used in the self-consistent calculations. The plane wave pseudopotential method based on VASP code is applied to calculate thermodynamic properties [43, 44].

## 3. Results and discussion

### 3.1. Stability

Firstly, we construct the structural model of CrHfCoZ (Z = Ga, In, Tl, Si) alloys, and discuss their site preference for each element as shown in Table I. It finds that the type I in total energies is the most stable structure. Further, we fit the data of energy-volume in order to get the ground states of CrHfCoZ alloys based on type I structure, the calculated equilibrium parameters are tabulated in Table II. Initially, we estimate the magnetic stability by comparing their total energy between ferromagnetic and nonmagnetic states for CrHfCoZ alloys before the presentation of electronic and magnetic properties. Results show that the ferrimagnetic configurations are more stable than the nonmagnetic one for all alloys. Based on the magnetic ground state, we calculate the formation energy $E_f$ to check the thermodynamics stability. For the quaternary Heulser alloys CrHfCoZ, the $E_f$ is defined as:

$$E_f = \frac{1}{4}\left[E_{\mathrm{CrHfCoZ}} - (E_{\mathrm{Cr}} + E_{\mathrm{Hf}} + E_{\mathrm{Co}} + E_{\mathrm{Z}})\right], \quad (1)$$

where $E_{\mathrm{CrHfCoZ}}$ are the total energies of the unit cell, the $E_{\mathrm{Cr}}$, $E_{\mathrm{Hf}}$, $E_{\mathrm{Co}}$ and $E_{\mathrm{Z}}$ are the their chemical potential. From the calculated $E_f$ shown in Table II, we can see that CrHfCoGa and CrHfCoSi alloys are likely to be synthesized in experiment because of their negative formation energy.

Further, the elastic constants $C_{ij}$ are calculated to verify the mechanical stability, the $C_{ij}$ can be obtained in the following formula:

$$C_{ij} = \frac{1}{V_0}\left(\frac{\partial^2 E}{\partial \varepsilon_i \varepsilon_j}\right), \quad (2)$$

where $E$ is the internal energy, $V_0$ is the equilibrium volume, and $\varepsilon_i$ or $\varepsilon_j$ denote applied strains. Only the $C_{11}$, $C_{12}$ and $C_{44}$ are independent of CrHfCoZ alloys, and they meet the mechanical stability conditions when the $C_{ij}$ obeys the Born–Huang criteria in the following

$$C_{11} + 2C_{12} > 0, \quad C_{11} - C_{12} > 0, \quad C_{44} > 0. \quad (3)$$

From the calculated $C_{ij}$ shown in Table II, we conclude that CoHfCoZ alloys satisfy the mechanical stability. Accordingly, the bulk modulus $B$, shear modulus $G$, Young's modulus $E$ and so on are also tabulated in Table II. Particularly, the $B/G$ is usually used to measure the brittleness and ductility of material. Here we predict that the CrHfCoZ alloys have a brittleness behavior.

TABLE I

The possible structures for quaternary Heusler alloys XX'YZ (CrHfCoZ) in different atomic arrangements.

| Structure | A(0,0,0) | B($\frac{1}{4}$, $\frac{1}{4}$, $\frac{1}{4}$) | C($\frac{1}{2}$, $\frac{1}{2}$, $\frac{1}{2}$) | D($\frac{3}{4}$, $\frac{3}{4}$, $\frac{3}{4}$) |
|---|---|---|---|---|
| type I | X | X' | Y | Z |
| type II | X' | X | Y | Z |
| type III | X | Y | X' | Z |

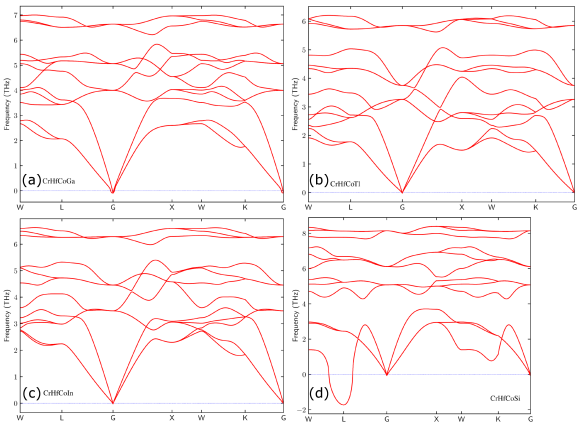


Fig. 1. Phonon dispersion curve for CrHfCoZ alloys at their equilibrium states.

In addition, we calculate the phonon spectrum of CrHfCoZ to evaluate their dynamics stability. From the calculated phonon spectrum shown in Fig. 1, we make a conclusion that CrHfCoZ alloys except for CrHfCoSi meet dynamic stability.

### 3.2. Electron orbital population and density of states

In Table III, the valence electrons of each atomic orbitals are provided for comparison with their outmost orbitals from the metals, the purpose is discussing the electron number transferred from one orbital to others or from one atom to others.

TABLE II

The calculated lattice parameters $a_{\mathrm{cal}}$ (in Åunit), elastic constants $C_{ij}$ (in GPa unit), bulk modulus $B$ (in GPa unit), shear modulus $G_{vrh}$, Young's modulus $E$ (in GPa unit), Poisson's ratio $\upsilon$, Pugh's indicator $B/G$, energy difference $\Delta E$ (in eV unit) between ferromagnetic and nonmagnetic states, and formation energy $E_f$ (in eV unit) for CrHfCoZ (Z=Ga, In, Tl, Si) alloys.

| Z | $a_{\mathrm{cal}}$ | $C_{11}$ | $C_{12}$ | $C_{44}$ | $B$ | $G_{vrh}$ | $E$ | $\upsilon$ | $B/G$ | $\Delta E$ | $E_f$ |
|---|---|---|---|---|---|---|---|---|---|---|---|
| Ga | 6.195 | 166.16 | 128.55 | 76.99 | 141.09 | 44.06 | 119.72 | 0.35 | 3.20 | −0.60 | −0.1374 |
| In | 6.419 | 169.62 | 115.94 | 74.98 | 133.84 | 49.69 | 132.65 | 0.33 | 2.69 | −0.73 | 0.0317 |
| Tl | 6.440 | 149.54 | 114.61 | 63.90 | 126.25 | 38.15 | 103.98 | 0.36 | 3.31 | −0.77 | 0.2386 |
| Si | 6.015 | 253.80 | 152.33 | 55.06 | 186.15 | 53.28 | 145.94 | 0.36 | 3.49 | −0.07 | −0.3389 |

TABLE III

Electron populations projected onto different atomic orbitals for CrHfCoZ (Z = Ga, In, Tl, Si) alloys.

| | | CrHfCoGa | CrHfCoIn | CrHfCoTl | CrHfCoSi |
|---|---|---|---|---|---|
| Cr (A) | 4*s* | 0.67 | 0.69 | 0.67 | 0.52 |
| | 3*d* | 4.79 | 4.80 | 4.81 | 0.52 |
| | 4*d* | 0.05 | 0.05 | 0.06 | 0.04 |
| | 4*p* | 0.65 | 0.64 | 0.63 | 0.51 |
| | Subtotal | 6.16 | 6.18 | 6.17 | 6.09 |
| Hf (B) | 6*s* | 0.61 | 0.66 | 0.65 | 0.54 |
| | 5*d* | 2.39 | 2.38 | 2.40 | 2.31 |
| | 6*d* | 0.03 | 0.04 | 0.05 | – |
| | 6*p* | 0.45 | 0.48 | 0.49 | 0.35 |
| | Subtotal | 3.48 | 3.56 | 3.59 | 3.20 |
| Co (C) | 4*s* | 0.8 | 0.8 | 0.78 | 0.69 |
| | 3*d* | 7.76 | 7.78 | 7.81 | 7.77 |
| | 4*d* | 0.18 | 0.18 | 0.18 | 0.16 |
| | 4*p* | 0.73 | 0.68 | 0.67 | 0.68 |
| | Subtotal | 9.47 | 9.44 | 9.44 | 9.30 |
| Z (D) | 3*s* | – | – | – | 1.34 |
| | 3*p* | – | – | – | 2.70 |
| | 3*d* | – | – | – | 0.41 |
| | 4*s* | 1.24 | – | – | – |
| | 4*p* | 1.63 | – | – | – |
| | 4*d* | 0.11 | – | – | – |
| | 5*s* | – | 1.12 | – | – |
| | 5*p* | – | 0.13 | – | – |
| | 5*d* | – | 1.68 | – | – |
| | 6*s* | – | – | 1.25 | – |
| | 6*p* | – | – | 0.1 | – |
| | 6*d* | – | – | 1.65 | – |
| | Subtotal | 2.98 | 2.93 | 3.0 | 4.45 |
| | Total | 22.09 | 22.11 | 22.20 | 23.04 |

It can be seen from Table III that 0.52 electrons for Hf atom and 0.02 electrons for Ga atom in CrHfCoGa are transferred to Cr atom and Co atom. The transferred valence numbers are 0.44 electrons for Hf atom and 0.03 electrons for In atom in CrHfCoIn, 0.42 electrons for Hf atom in CrHfCoTl, 0.88 electrons for Hf atom in CrHfCoSi, respectively. For the Co, Hf, and Cr atoms, there are electrons partially transferred to the Hf 5*d* and Co 3*d* orbitals, and some of Cr 3*d* electrons are probably transferred, the *p* electrons are mainly transferred for Z atom, the other part are left. These transferred electrons lead to the mixture of *d* orbital wave function and electronegativity, accordingly, also indicating these states participate in the bonding. In addition, it should be in mind that the appearance of Cr 4*d*, Hf 6*d*, Co 4*d*, and Z *d* electrons will improve the completeness of basis set and accuracy of calculations, they do not make sense in physics.

In order to understand the electronic behaviors, we analyze the total and resolved density of states (DOS) in Fig. 2. It is evident that a band gap is observed at the Fermi level for all alloys in one spin channel, while there is an existence of DOS in the other spin channel, suggesting their half-metallic nature. Particularly, the gap is

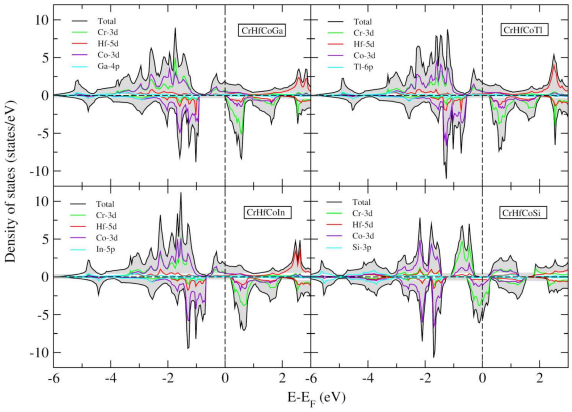


Fig. 2. Spin-dependent total and orbital-resolve density of states of CrHfCoZ alloys.

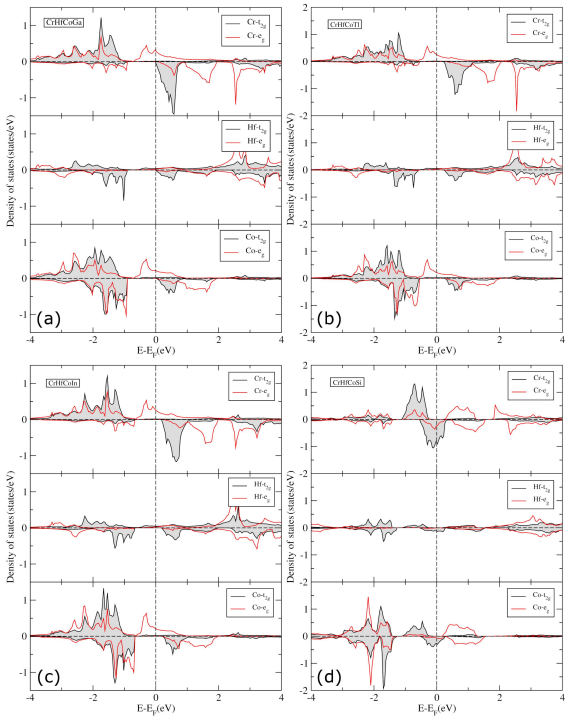


Fig. 3. Spin-dependent local density of states for CrHfCoZ alloys.

pinned in minority-spin for CrHfCoGa, CrHfCoIn and CrHfCoTl alloys, and it is majority-spin for CrHfCoSi alloy. In addition, the strong hybridizations between the Cr 3*d* and Co 3*d* states lead to an energy distribution spreading from −4 eV to 1 eV for these alloys, which is also confirmed by electron orbital population. The Cr 3*d* electrons govern the −1 to 1 eV interval, the other *d* states almost offer the same contribution to overall DOS. For the *p* electrons, the contribution is rather small for overall DOS, while it offers a *p*–*d* orbital occupation, which stabilizes these systems. The formation of gap ascribes to the exchange splitting of $t_{2g}$–$e_g$ states, also seen from the local density of states (LDOS) in Fig. 3. Among them, the exchange

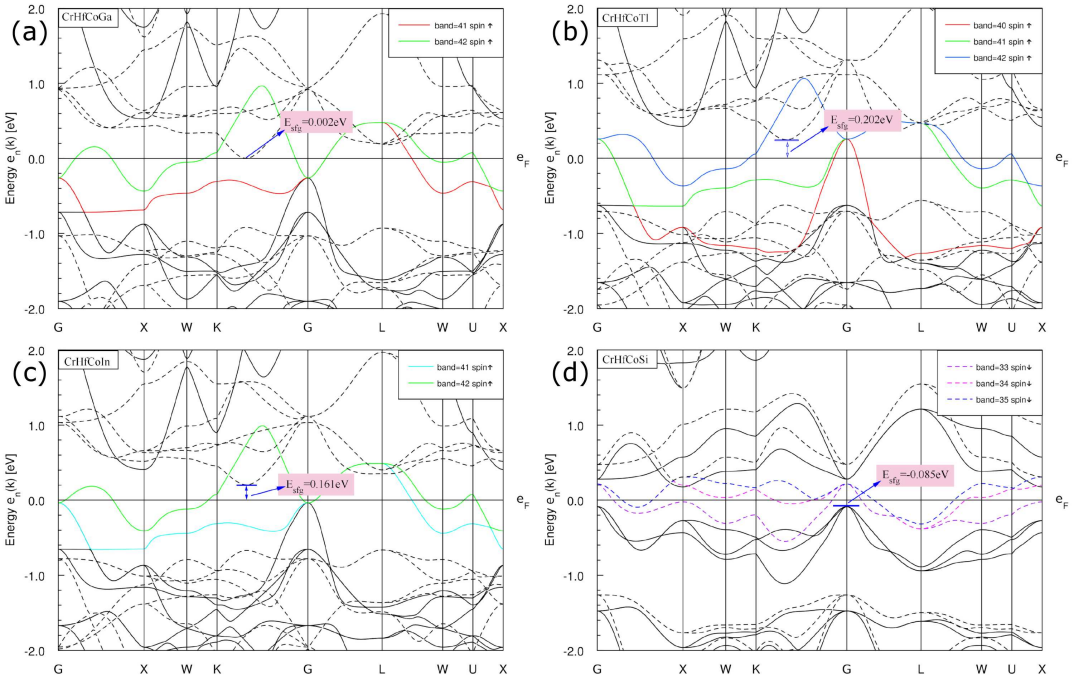


Fig. 4. Band structures for CrHfCoZ alloys are shown. Note that the valence bands are highlighted.

splitting of $t_{2g}$ and $e_g$ states for Cr and Co atoms is obvious than one of Hf atom, actually it is well consistent with their calculated magnetic moments. Calculated spin-flip gap is also labeled in band pictures in Fig. 4, it finds the CrHfCoTl alloy has largest half-metallic gap up to 0.202 eV, indicating its most stable half-metallic properties, while for the CrHfCoGa and CrHfCoSi alloys, the spin-flip gap almost closes to zero, also implying their unstable half-metallic properties to other alloys.

### 3.3. Magnetic moments and orbital occupation

Now, we focus on the magnetic moments of CrHfCoZ alloys, as expected, the CrHfCoZ have an integer spin magnetic moments per unit cell since their valence electrons can be viewed as itinerant ones. In all alloys, the Cr magnetic moment offers a main contribution for total magnetic moment as seen in Table IV. It is identical with its DOS, namely the spin-up electron governs occupied states around the Fermi level, and its sign is consistent with Co moment, and opposite with Z moment. The contribution of Z moment to overall is rather small because of its unpolarized, especially, the Hf moment in CrHfCoSi is parallel to Cr moment. Therefore, CrHfCoZ alloys can be treated as ferrimagnetic half-metals. In fact, the CrHfCoSi is also seen as ferromagnet owing to its smaller Si magnetic moment. Further, the total magnetic moments 4 $\mu_B$ for CrHfCoGa, CrHfCoIn and CrHfCoTl alloys as well as 1 $\mu_B$ for CrHfCoSi alloy obey the Slater–Pauling rule $M_t = Z_t - 18$, where $M_t$ denotes total magnetic moments (in $\mu_B$ units) and $Z_t$ denotes total valence electron number. Actually, the total magnetic moment $M_t$ equals to $N\uparrow - N\downarrow$, where the $N\uparrow$ is spin-up valence electrons number, and the $N\downarrow$ is spin-down valence electrons number, and the $Z_t$ equals to $N\uparrow + N\downarrow$, and then $M_t = Z_t - 2N\downarrow$. In order to obtain the occupied valence electrons states, we offer the $d$–$d$ hybridizations under crystal field in Fig. 5. At the begging, the $d$-orbitals between Cr and Co atoms hybridize with each other because of their same octahedral symmetry, then creating five bonding $t_{2g}$ states with triple-degeneracy and $e_g$ states with double-degeneracy, and five non-bonding $t_{1u}$ states with triple-degeneracy and $e_u$ states with degeneracy. In turn, the five bonding $d$-hybrids hybridize with the Hf $d$ orbitals due to the same tetragonal symmetry, and then creating again bonding and antibonding states. Moreover, a single $s$ state and a $p$ states with triple-degeneracy are provided by the Z element, and they partially accommodate $d$-charge from the Cr, Hf and Co atoms as discussed in orbital population. Finally, there are nine occupied states in minority-spin, i.e., $N\downarrow = 9$, including the triple-degenerated $t_{2g}$, double-degenerated $e_g$, and triple-degenerated $p$ and a single $s$ states, respectively, thus the total magnetic moments follow the $M_t = Z_t - 18$ rule. Actually, the mechanism, leading to the Slater–Pauling rule, is also discussed in Refs. [45, 46].

### 3.4. Fermi properties and effect of lattice

To further understand the characters of electrons, detailed valence band pictures and Fermi surface are given. In Fig. 4, we show the energy band dispersions pictures in the vicinity of Fermi energy, and highlighted the valence bands. Here we find two valence bands crossing the Fermi energy

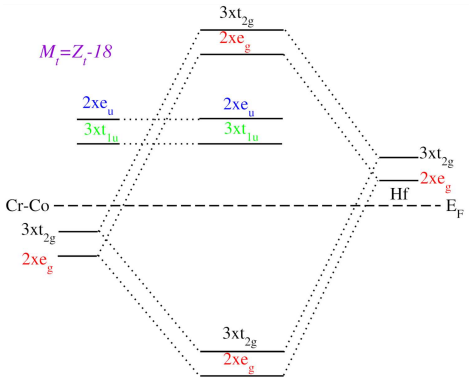


Fig. 5. Calculated Fermi surface with extremal orbits is indicated for CrHfCoZ alloys.

TABLE IV

Calculated total ($M_t^{\rm tot}$) and atomic magnetic moments (in $\mu_{\rm B}$ unit) for CrHfCoZ (Z = Ga, In, Tl, Si) alloys.

| Alloys | $M_t^{\rm tot}$ | Cr | Hf | Co | Z |
|---|---|---|---|---|---|
| CrHfCoGa | 4.00 | 3.553 | −0.217 | 0.807 | −0.143 |
| CrHfCoIn | 4.00 | 3.694 | −0.292 | 0.764 | −0.166 |
| CrHfCoTl | 4.00 | 3.727 | −0.302 | 0.731 | −0.157 |
| CrHfCoSi | 1.00 | 1.040 | 0.016 | 0.017 | −0.073 |

of CrHfCoGa and CrHfCoIn alloys, these bands are denoted as spin-up 41 and 42 numbers. The spin-up 40, 41 and 42 bands cross the Fermi energy for the CrHfCoTl alloy. It becomes spin-down 33, 34, and 35 bands for CrHfCoSi, the band number is labeled according to their valence band complex in the scalar relativistic calculation. The bands 41 and 42 for CrHfCoGa, CrHfCoIn, and CrHfCoTl alloys are degenerate between $\Gamma$ and $L$ symmetry points, indicating their characteristics of conduction bands, and the degeneracy is lifted in other directions. Specially, the bands 33 and 34 for CrHfCoSi are also degenerate between $\Gamma$ and $L$ and $\Gamma$ and $X$ high symmetry points, indicating the electron behavior. In Fig. 6, the Fermi surface is shown to argue valence bands, for the CrHfCoGa and CrHfCoIn alloys, a open spiral cone Fermi surface is indicated, and the band 41 shows electron-like behavior, and it is hole-like behavior for band 42. As for CrHfCoTl alloy, the 40 band is closed polyhedron shape, indicating electron-like nature, also for band 41, while the band 42 shows the shape of cone, indicating hole-like behavior. More particularly, the band 33 shows closed polyhedron shape, while 34 and 35 bands are hole-like behavior, indicating a bowl shape. Finally, we give the changes of conduction band minimum (CBM) and valence band maximum (VBM) dependent on lattice constants in Fig. 7, since the half-metals usually can be grown as thin films on the substrates, which makes the lattice constants deviation from equilibrium constants. From Fig. 3, we notice that the CBM and VBM

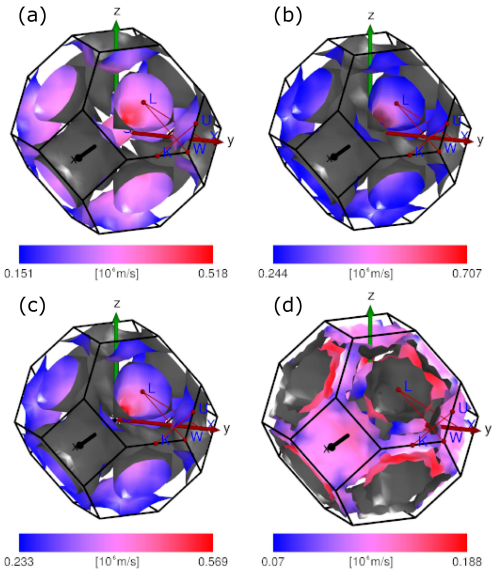


Fig. 6. Hybridizations between $d$-orbitals sitting at different sites for CrHfCoZ alloys. The coefficient represents the degeneracy of each orbital.

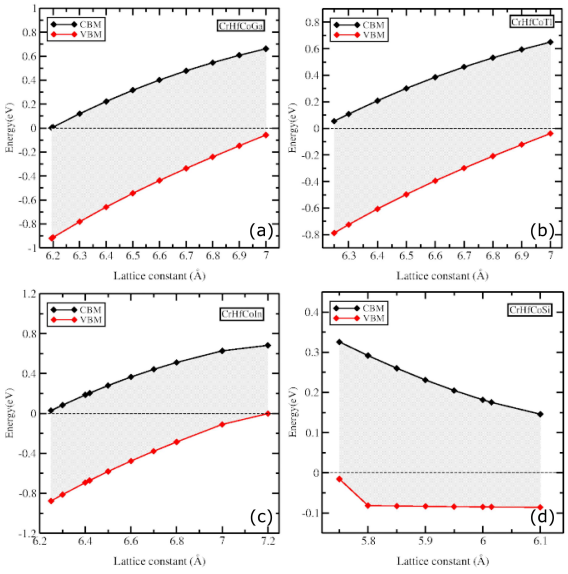


Fig. 7. Changes of valence band maximum and conduction band minimum for CrHfCoZ dependent on lattice constants.

becomes gradually bigger as the increase of lattice constants due to the rigid band model. While for the CrHfCoSi alloy, the VBM decreases with the increase of lattice constants, and the VBM decrease quickly, then keeping nearly the constant. Therefore, we can tune the spin-flip gap by engineering the lattice constants.

## 4. Summary and conclusions

Electronic calculations show that the CrHfCoZ alloys are half-metallic ferrimagnets. Negative formation energies in CrHfCoAl and CrHfCoSi alloys

indicate that they are likely synthesized in experiment. Calculated elastic constants for all alloys meet mechanical stability condition. The CrHfCoZ apart from CrHfCoSi satisfy thermodynamic stability according to the phonon spectrum. A strong *d*-*d* orbital hybridizations are observed from electron population and density of states, and lead to the formation of gap. More detail, the gap ascribes to the $t_{2g}$–$e_g$ exchange splitting according to the local density of states. The total integral magnetic moments of CrHfCoZ, which follows the Slater–Pauling $M_t = Z_t - 18$, are also discussed by the electronic occupation under crystal field. In addition, the VBM and CBM dependent on lattice parameters are also shown. The current research may offer some valuable hints for these alloys in spintronic applications.

## Acknowledgments

The work is supported by National Natural Science Foundation of China (No. 11864021), the work is also supported by Foundation of A Hundred Youth Talents Training Program of Lanzhou Jiaotong University, and the Excellent Research Team of Lanzhou Jiaotong University, China (Grant No. 201803). In addition, the work is also supported by the Key Talent Foundation of Gansu Province.

## References

[1] R.A. de Groot, F.M. Mueller, G.P. van Engen, K.H.J. Buschow, *Phys. Rev. Lett.* **50**, 2024 (1983).

[2] K. Schwarz, *J. Phys. F Met. Phys.* **16**, L211 (1986).

[3] M.A. Korotin, V.I. Anisimov, D.I. Khomskii, G.A. Sawatzky, *Phys. Rev. Lett.* **80**, 4305 (1998).

[4] A. Yanase, K. Siratori, *J. Phys. Soc. Jpn.* **53**, 312 (1984).

[5] S. Soeya, J. Hayakawa, H. Takahashi, K. Ito, C. Yamamoto, A. Kida, H. Asano, M. Matsui, *Appl. Phys. Lett.* **80**, 823 (2002).

[6] Y.P. Liu, S.H. Chen, J.C. Tung, Y.K. Wang, *Solid State Commun.* **152**, 968 (2012).

[7] K.I. Kobayashi, T. Kimura, H. Sawada, K. Terakura, Y. Tokura, *Nature* **395**, 677 (1998).

[8] O. Erten, O. Nganba Meetei, A. Mukherjee, M. Randeria, N. Trivedi, P. Woodward, *Phys. Rev. B* **87**, 165105 (2013).

[9] O. Erten, O. Nganba Meetei, A. Mukherjee, M. Randeria, N. Trivedi, P. Woodward, *Phys. Rev. Lett.* **107**, 257201 (2011).

[10] S. Chen, J. Zhou, Z.M. Sun, *ACS Appl. Mater. Interfaces* **7**, 31 (2015).

[11] J.J. He, P.B. Lyu, P. Nachtigall, *J. Mater. Chem. C* **4**, 11143 (2016).

[12] Y. Zhang, F. Li, *J. Magn. Magn. Mater.* **433**, 222 (2017).

[13] G. Wang, *J. Phys. Chem. C* **120**, 33 (2016).

[14] S.S. Li, S.J. Hu, W.X. Ji, P. Li, K. Zhang, C.W. Zhang, S.S. Yan, *Appl. Phys. Lett.* **111**, 202405 (2017).

[15] G. Wang, Y. Liao, *Appl. Surf. Sci.* **426**, 80 (2017).

[16] G.Y. Gao, G.Q. Ding, J. Lie, K.L. Yao, M.H. Wu, M.C. Qian, *Nanoscale* **8**, 8986 (2016).

[17] G.D. Liu, X.F. Dai, H.Y. Liu, J.L. Chen, Y.X. Li, G. Xiao, G.H. Wu, *Phys. Rev. B* **77**, 014424 (2008).

[18] K. Özdoğan, E. Şaşıoğlu, B. Aktaş, and I. Galanakis, *Phys. Rev. B* **74**, 172412 (2006).

[19] H.Z. Luo, G.D. Liu, F.B. Meng, J.Q. Li, E.K. Liu, G.H. Wu, *J. Magn. Magn. Mater.* **324**, 3295 (2012).

[20] Xiao-Ping Wei, Jian-Bo Deng, Ge-Yong Mao, Shi-Bin Chu, Xian-Ru Hu, *Intermetallics* **29**, 86 (2012).

[21] H.M. Huang, S.J. Luo, K.L. Yao, *J. Magn. Magn. Mater.* **324**, 2560 (2012).

[22] V. Alijani, J. Winterlik, G.H. Fecher, S. Shahab Naghavi, C. Felser, *Phys. Rev. B* **83**, 184428 (2011).

[23] H.Z. Luo, G.D. Liu, F.B. Meng, L.L. Wang, E.K. Liu, G.H. Wu, X.X. Zhu, C.B. Jiang, *Comput. Mater. Sci.* **50**, 3119 (2011).

[24] X.P. Wei, S.B. Chu, G.Y. Mao, H. Deng, T. Lei, X.R. Hu, *J. Magn. Magn. Mater.* **323**, 2295 (2011).

[25] A. Birsan, P. Palade, V. Kuncser, *J. Magn. Magn. Mater.* **331**, 109 (2013).

[26] X.F. Zhu, Y.X. Wang, L. Wang, Y.F. Dai, C.L. Luo, *J. Phys. Chem. Solids* **75**, 391 (2014).

[27] F. Lei, C.C. Tang, S.J. Wang, W.C. He, *J. Alloys Compd.* **509**, 5187 (2011).

[28] F. Ahmadian, *J. Alloys Compd.* **576**, 279 (2013).

[29] J. Drews, U. Eberz, H. Schuster, *J. Less-Common Met.* **116** (1986) 271.

[30] X. Dai, G. Liu, G.H. Fecher, C. Felser, Y. Li, H. Liu, *J. Appl. Phys.* **105**, 07E901 (2009).

[31] G.Y. Gao, L. Hu, K.Y. Yao, B. Luo, N. Liu, *J. Alloys Compd.* **551**, 539 (2013).

[32] A. Kundu, S. Ghosh, R. Banerjee, S. Ghosh, B. Sanyal, *Sci. Rep.* **7**, 1803 (2017).

[33] L. Xiong, L. Yi, G.Y. Gao, *J. Magn. Magn. Mater.* **360**, 98 (2014).

[34] S. Berri, D. Maouche, M. Ibrir, F. Zerarga, *J. Magn. Magn. Mater.* **354**, 65 (2014).

[35] D. Rani, L. Bainsla, K.G. Suresh, A. Alam, *J. Magn. Magn. Mater.* **492**, 165662 (2019).

[36] I. Muhammad, J.M. Zhang, A. Ali, M.U. Rehman, S. Muhammad, *Thin Solid Films* **690**, 137564 (2019).

[37] B. Wu, H.S. Huang, G.D. Zhou, X.D. Yang, P. Li, Y. Feng, *Eur. Phys. J. B* **92**, 119 (2019).

[38] S. Idrissi, S. Ziti, H. Labrim, L. Bahmad, I. El Housni, R. Khalladi, S. Mtougui, N. El Mekkaoui, *J. Alloys Compd.* **820**, 153373 (2020).

[39] Z. Cui, B. Wu, X. Ruan, Q.W. Zhou, Z.Y. Liu, X.Y. Fu, Y. Feng, *Results Phys.* **15**, 102533 (2019).

[40] K. Koepernik, H. Eschrig, *Phys. Rev. B* **59**, 1743 (1999).

[41] I. Opahle, K. Koepernik, H. Eschrig, *Phys. Rev. B* **60**, 14035 (1999).

[42] J.P. Perdew, K. Burke, M. Ernzerhof, *Phys. Rev. Lett.* **77**, 3865 (1996).

[43] G. Kresse, J. Furthmuller, *Phys. Rev. B* **54**, 11169 (1996).

[44] G. Kresse, D. Joubert, *Phys. Rev. B* **59**, 1758 (1999).

[45] S. Skaftouros, K. Özdoğan, E. Şaşıoğlu, I. Galanakis, *Phys. Rev. B* **87**, 024420 (2013).

[46] K. Özdoğan, E. Şaşıoğlu, I. Galanakis, *J. Appl. Phys.* **113**, 193903 (2013).